Physicochem. Probl. Miner. Process., 60(1), 2024, 185550

http://www.journalssystem.com/ppmp

Physicochemical Problems of Mineral Processing

ISSN 1643-1049

Flotation performance of a novel collector, ethyl o-mesitylsulfonylacetohydroxamate, for bastnaesite ores

Yuli Di, Xiankui Liu, Xia He, Hao Zhang, Haiyan Huang, Cheng Wang and Yu Jiao

College of Science, Xichang University, Xichang 615000, China

Corresponding author: xcc02900034@xcc.edu.cn (Yu Jiao)

Abstract: Existing collectors used in the flotation process of bastnaesite ores are characterized by the poor flotation performance and low recovery. In this paper, from the perspective of molecular structure, ethyl O-mesitylsulfonylacetohydroxamate (C_1) was selected as a novel collector for bastnaesite ores, and compared with the most commonly used collector, salicylhydroxamic acid (C_2), in the flotation test with bastnaesite ore with fine mineral particles, complex embedding and a high mud content. The flotation test confirmed that C1 had the better collection ability and flotation performance than C_2. Then, the adsorption mechanisms between collectors (C_1 and C_2) and bastnaesite surface were explored based on first principles thinking. The adsorption energies between collectors (C_1 and C_2) and the (110) plane of bastnaesite were respectively calculated as -1.79 eV and -1.44 eV and corresponding adsorption heights were respectively 1.65 Å and 2.43 Å. These data indicated that C_1 had the better affinity to the (110) plane of bastnaesite and the better binding. The calculation results of partial density of states (PDOS) showed that both collectors underwent significant orbital hybridization with the (110) plane of bastnaesite, suggesting strong electronic interactions.

Keywords: bastnaesite ore, flotation, density functional theory, surface adsorption

1. Introduction

Bastnaesite ore is one of the most important minerals of rare earth cerium and mainly distributed in alkaline rocks, alkaline pegmatites and related hydrothermal mineral deposits (Anderson, 2021; Boulanger et al., 2019). Most of the bastnaesite ores are finely embedded particles with complex embedding relationships with other minerals, high contents of associated minerals such as fluorite, barite, strontium-barium sulfate minerals, and serious ore mudification, thus largely increasing the recycling difficulty of rare earth minerals (Bolonin, 2018; Xu et al., 2020a).

Currently, most of bastnaesite ores are processed with a combined process of magnetic separation (Park et al., 2021; Wang et al., 2020a; Wang et al., 2020b; Xiong et al., 2018) and flotation (Duan et al., 2020b; Wang et al., 2023; Wang et al., 2020c; Zhou et al., 2023; Zhu et al., 2020) to produce rare earth concentrates. Flotation is a selective screening process of minerals to separate and float different minerals based on the hydrophilic/hydrophobic nature of collector molecules and the difference in the affinity to the surface of different minerals. Flotation is an important beneficiation method for bastnaesite ores at present (Guo et al., 2022a; Liu et al., 2024; Liu et al., 2019; Wang et al., 2020d; Wang et al., 2020e). The grade and yield of rare earth concentrates obtained by flotation are influenced by flotation conditions such as grinding fineness, type of collector, dosage of inhibitor, and flotation parameters (Liu et al., 2018; Liu et al., 2016). A collector is one of the most important agents in flotation since it directly determines the performance of flotation method and plays an extremely critical role in the rare earth recovery and concentrate grade. Therefore, efficient collectors for bastnaesite have been widely concerned and explored (Duan et al., 2020a; Fan et al., 2021; Xu et al., 2020a; Xu et al., 2020b). However, the studies on the selection of collector molecules and their microscopic interaction mechanism with bastnaesite surface were seldom reported and still in the trial-and-error stage (Guo et al., 2022b; Xu et al., 2022).

DOI: 10.37190/ppmp/185550

The collection process of bastnaesite by collectors involves two abilities, namely the ability of adsorption on mineral surfaces and the ability to increase the hydrophobicity of mineral surfaces(Hu et al., 2021; Kang and Liu, 2021). Therefore, the molecule as a rare earth mineral collector should have a functional group that can be adsorbed on mineral surfaces and a functional group that can make the mineral surface hydrophobic. In short, it is necessarily composed of a polar group (also called solid-philic group) and non-polar group (or hydrophobic group). Ce^{3+} ions in bastnaesite ($Ce(CO_3)F$) contain unfilled 4f electrons (Cao et al., 2020) and large rare earth ions are easily combined with ligand atoms due to electrostatic attraction. According to the acid-base classification method, rare earth ions belong to the group of hard acids and have a strong coordination ability with coordination atoms belonging to hard bases, such as oxygen, fluorine, and nitrogen, and a weak coordination ability with coordination atoms belonging to weak bases, such as sulfur and phosphorus (Liu and Chen, 2021; Zhang et al., 2022)

Increasing the hydrophobic property of the collector molecule can enhance its collection ability (Liu et al., 2021; Sun et al., 2021), but the selectivity of a collector for bastnaesite depends on the interaction force between the collector molecule and the mineral. Ethyl O-mesitylsulfonylacetohydroxamate with the structural formula of $(CH_3)_3C_6H_2SO_3NC(CH_3)OCH_2CH_3$ is a nonionic molecule with a weakly polar benzene ring with a methyl group and good hydrophobicity. In addition, this compound has multiple electron pair donors of O and N, and trimethyl benzene ring which can increase the electron density of electron donors. If O and N in the molecule form the coordination bond with Ce^{3+}, a stable five-membered ring can be formed after coordination. Theoretical analysis results indicate that ethyl O-mesitylsulfonylacetohydroxamate (C_1) has the good adsorption and collection performance for bastnaesite. Therefore, in this study, with salicylhydroxamic acid (C_2) commonly used in the beneficiation production of bastnaesite as a comparative collector, the flotation test of bastnaesite reported in our previous study(Jiao et al., 2020) was performed to explore the collection (Wang et al., 2021; Yu et al., 2021; Zhang et al., 2021) performance of C_1. Based on the application of first principles thinking in flotation (Gong et al., 2021; Nie et al., 2020; Quezada and Toledo, 2019; Sahraei and Larachi, 2020; Yao et al., 2021), the adsorption energy, adsorption height, and partial density of states (PDOS) of two collectors (C_1 and C_2) on bastnaesite surface (the (110) plane) were calculated to reveal the microscopic mechanism for the actions of collector molecules on mineral surface. The results showed that the collector C_1 had good application prospects in the flotation process of bastnaesite ore.

2. Materials and methods

2.1. Materials and instruments

Nitric acid (HNO_3), hydrochloric acid (HCl), perchloric acid ($HClO_4$), oxalic acid($H_2C_2O_4$), ammonium chloride(NH_4Cl), and ammonia are analytically pure products purchased from Chengdu Kelong Chemical Co., Ltd. Salicylic hydroxamic acid (99.5%, C_2), Ethyl O-mesitylsulfonylacetohydroxamate (99.9%, C_1), water glass (modulus, 2.8), and turpentine oil (2# oil) was purchased from Chengdu Ouenreisi Chemical Reagent Co., Ltd. Bastnaesite ore was provided by a mine in Sichuan.

An X-ray fluorescence spectrometer (XRFl800F, Shimadzu, Japan) was used to characterize the elements contained in the minerals and semi-quantify the content of each oxide. The automated mineral identification and characterization system (AMICS) (Sigma 500, Germany Zeiss) was used to determine element composition, phase composition, particle size distribution, embedding state and liberation degree of minerals. A ball mill (XQM2L, Tianjin Hongyang Machinery Equipment Co., Ltd.) was used to reduce mineral fineness. A single-cell flotation machine (1 L, Shaoxing Shangyu Jinfeng Machinery & Instruments Co., Ltd.) was used in the flotation test.

2.2. Experimental process

Beneficiation test was performed according to the following steps. Bastnaesite ore provided by a certain mine in Sichuan was firstly crushed to a particle diameter of -15 mm by jaw crusher and particles with the diameter less than 15 μm were screened. Then, large particles were further ball-milled until remaining particles with a diameter of 75 μm accounted for 82%. Then, the ball-milled particles were used for flotation. The beneficiation test process is shown in Fig. 1.

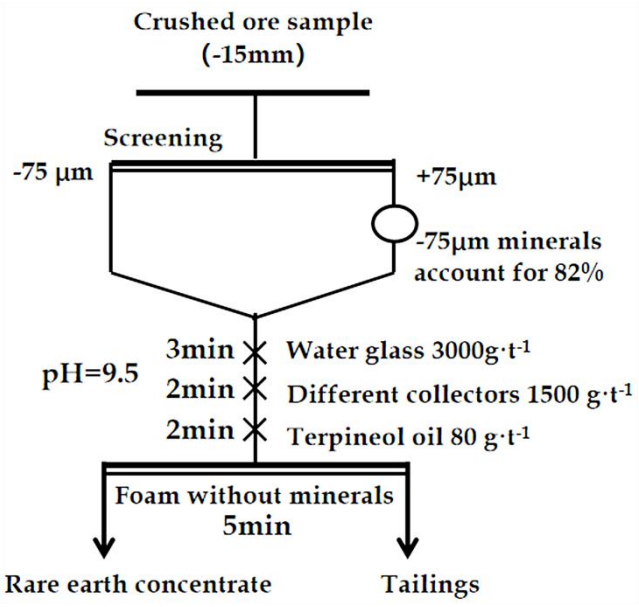

Fig. 1. Flow diagram of the beneficiation test

Flotation test was carried out according to the following steps. Firstly, 300 g of bastnaesite particles was mixed with 850 g of water to obtain the mineral slurry and pH was adjusted to 9.5 with sodium hydroxide (NaOH). Under the conditions of room temperature, aeration rate of 0.35 m^3/h, and stirring speed of 3000 r/min, inhibitor (water glass), collector (C_1 or C_2), and frothing agent (2# oil) were added in sequence and then water was added to a given volume. Under stirring conditions, a lot of foam was formed and bastnaesite concentrate was scraped out together with foam. In addtion, the conditioning (2 min) and scrapping times (5 min) were determained based on other literature (Duan et al., 2020a; Lin et al., 2020). Water was continuously supplied so that foam could be scraped out. The flotation process is shown in Fig. 2. The collected froth products were dried at 105 ° C for 24 h after vacuum filtration and then the grade of the obtained rare earth concentrate was determined according to GBT 14635-2020 (Repub and Regulation, 2020).

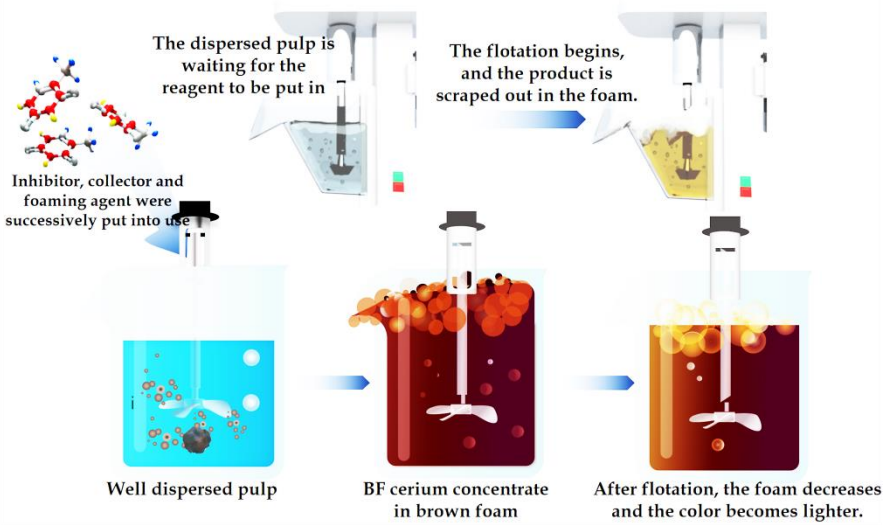

Fig. 2. Schematic diagram of the flotation process

2.3. Computational details

Parameters were calculated according to the following method. All calculations were conducted in the Cambridge sequential total energy package (CASTEP) program of Materials Studio software based on DFT(Segall et al., 2002). This program provides an effective implementation of DFT plane-wave (PW)

pseudopotential method to investigate the various properties and geometry of adsorbate and surface systems. The widely used generalized gradient approximation (GGA) and Perdew-Burke-Ernzerhof (PBE) were used to describe the exchange-correlation interactions (Ernzerhof et al., 1996; Y. and W., 1998). The spin polarized approximation was considered throughout all calculation and electro-ion interactions was described using Ultra-soft pseudopotential. For geometry optimization, the energy tolerance was set as 0.001eV/ cell, and maximum force tolerance was set as 100 eV/Å. A pre-tested plane wave dynamic cutoff energy of 370 eV was used to obtain high-quality results for all calculations. The Brillouin zone was sampled using a Gamma point due to 90~110 atoms were used in the unit cell. In addition, in order to ensure the accuracy of calculation, the above parameters are same when calculating energy and other properties.

3. Results and discussion

3.1. Properties of bastnaesite ore

Before flotation, it is necessary to analyze the chemical composition, oxide content, and phase composition of the ore in order to provide a basis for the ore selectivity test.

3.1.1. Chemical composition and oxide content of the ore

The chemical composition and content of bastnaesite sample were determined by XRF test (Table 1). According to Table 1, the bastnaesite sample mainly contains three rare earth elements: Ce, La, and Nd. It can be seen that the contents of CeO_2, La_2O_3, and Nd_2O_3 were 2.72%, 1.85%, and 0.66%, respectively. Therefore, the content of TREO was 5.23% (2.72+1.85+0.66). The low contents of rare earth in the sample further increased the difficulty of mineral beneficiation. The non-rare earth element in the ore sample were mainly Ca and Sr, so the flotation process focused on removing calcium-bearing and strontium-bearing gangue minerals.

Table 1. XRF analysis results of element composition and oxide content of bastnaesite sample from a mining area (wt/%) (TREO is an abbreviation for Total Rare Earth Oxides)

component	CeO_2	La_2O_3	Nd_2O_3	TREO	F	CaO	SrO
Content（wt/%）	2.72	1.85	0.66	5.23	9.97	41.03	22.07
component	SO_3	SiO_2	BaO	Al_2O_3	Fe_2O_3	K_2O	other
Content（wt/%）	5.81	5.65	5.13	1.76	1.27	0.23	1.85

3.1.2. Mineral composition and structure of the ore

There is no other rare earth minerals were detected in samples. Therefore, we focused on testing bastnaesite ore. Fig. 3 shows the SEM image of the different bastnaesite samples. The AMICS analysis results indicated that the diameter of most of bastnaesite ore particles was less than 50 μm. Gangue minerals are mainly feldspar, calcite, quartz, azurite, fluorite, barite, etc. Bastnaesite and gangue minerals formed the association, interlocking, or inclusion relationship, displaying the serious intergrowth relationship with feldspar, calcite, quartz, fluorite, and black mica. Ore particles were small and many associated minerals existed. The ore structure was complex, thus leading to the difficulty in beneficiation.

3.2. Flotation test results of C_1 and C_2

With C_1 or C_2 as the collector, the flotation of raw bastnaesite was respectively performed according to the process shown in Fig. 1. The flotation results are shown in Table 2 (The REO grade was determined by EDTA titration method in GBT 14365-2020) .

With C_1 as collector, the flotation gave concentrate yield of 16.49% together with the grade and recovery rate of concentrate reaching 21.18% and 66.78%, respectively (Table 2). When C_2 was used as collector, the concentrate yield reached 19.02% and the grade and recovery rate of concentrate were of 15.36% and 55.86%, respectively.

Table 2. Flotation results respectively obtained with C_1 and C_2.

Collector	Product	Yield/%	Grade /% REO	Recovery rate /% REO
	concentrate	16.49	21.18	66.79
C_1	tailings	83.51	2.08	33.21
	Ore feeding	100.00	5.23	100.00
	concentrate	19.02	15.36	55.87
C_2	tailings	80.98	2.85	44.13
	Ore feeding	100.00	5.23	100.00

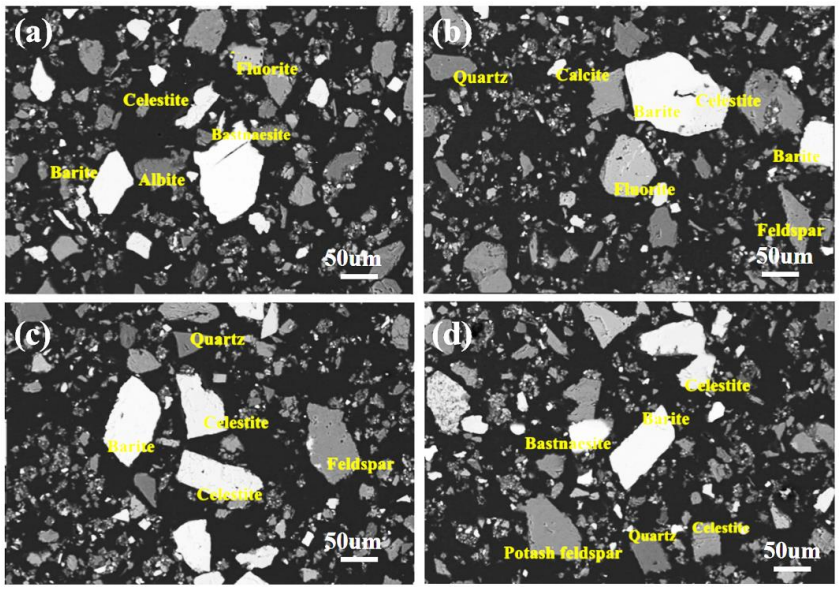

Fig. 3. SEM image of different bastnaesite sample

3.3. Mechanism of the interaction between the collector and bastnaesite ore

The results flotation test indicated that C_1 as a collector had the better selectivity and collection performance of bastnaesite ore than C_2. In order to further analyze the inherent mechanism for the difference in the flotation effect between C_1 and C_2, the adsorption energy, adsorption height and PDOS of C_1 and C_2 on the (110) plane of bastnaesite crystals were calculated based on first principles thinking.

3.2.1. Chemical properties of the (110) plane of bastnaesite crystals

The structure of bastnaesite crystal (Fig. 4(a)) was imported from the inorganic crystal structure database. The crystal structure of low energy state was obtained by calculation and then optimized to yield the crystal structure of bastnaesite (Fig. 4(b)). Lattice parameters and corresponding bond lengths of the optimized crystal structure were listed in Table 3.

Table 3. Lattice parameters and corresponding bond lengths of bastnaesite crystal before and after optimization

Bastnaesite crystal	Bond length *l* before optimization (Å)	Bond length *l* after optimization (Å)
a=b	7.14	7.19
c	9.81	7.89
$l_{F\text{-}Ce}$	2.43	2.46
$l_{O\text{-}Ce}$	2.58	2.63
$l_{F\text{-}O}$	3.19	3.20
$l_{F\text{-}C}$	3.29	3.32
$l_{C\text{-}Ce}$	3.24	3.30
$l_{O\text{-}C}$	1.34	1.30

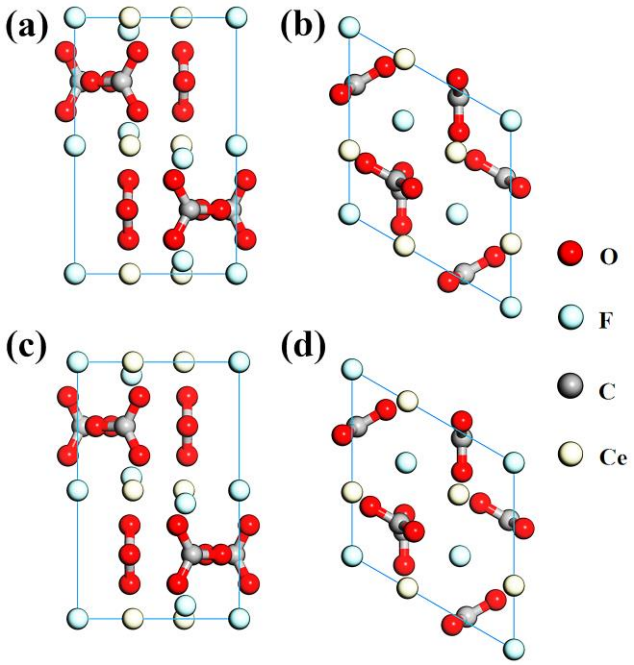

Fig. 4. Main and top views of the crystal cell of bastnaesite (a,b) before and after (c,d) optimization (Red, sky blue, grey and light yellow represent oxygen, fluorine, carbon and cerium atoms, respectively. Table 1 shows that bastnaesite contains La and Nd elements, but the content of these two elements are relatively low and cannot be plotted in a unit crystal cell

As shown in Table 3, the relaxed lattice parameters are respectively: a = b = 7.19 Å, c = 7.89 Å, and $\gamma = 120^{\circ}$, which are close to the reported values (Ni et al., 1993). It also indicated that the parameters used in the calculation were reasonable. Compared to the structure before optimization, the optimized structure showed slight expansion. In addition, the bond lengths of $l_{F\text{-}Ce}$, $l_{O\text{-}Ce}$, $l_{F\text{-}O}$, $l_{Ce\text{-}C}$, and $l_{F\text{-}C}$ increased after optimization (Fig. 4(b), Table 3). The results were consistent with the lattice change. However, the bond length $l_{O\text{-}C}$ decreased. The bond lengths and changes were almost consistent with the previous report(Donnay and Donnay, 1953). In order to analyze the hybridization among individual atomic orbits in bastnaesite, the PDOS of bastnaesite crystal cell was calculated (Fig. 5(a)). For visualizing the charge distribution of individual atoms and the bonds among atoms, the charge density difference diagram of bastnaesite was further calculated (Fig. 5(b)).

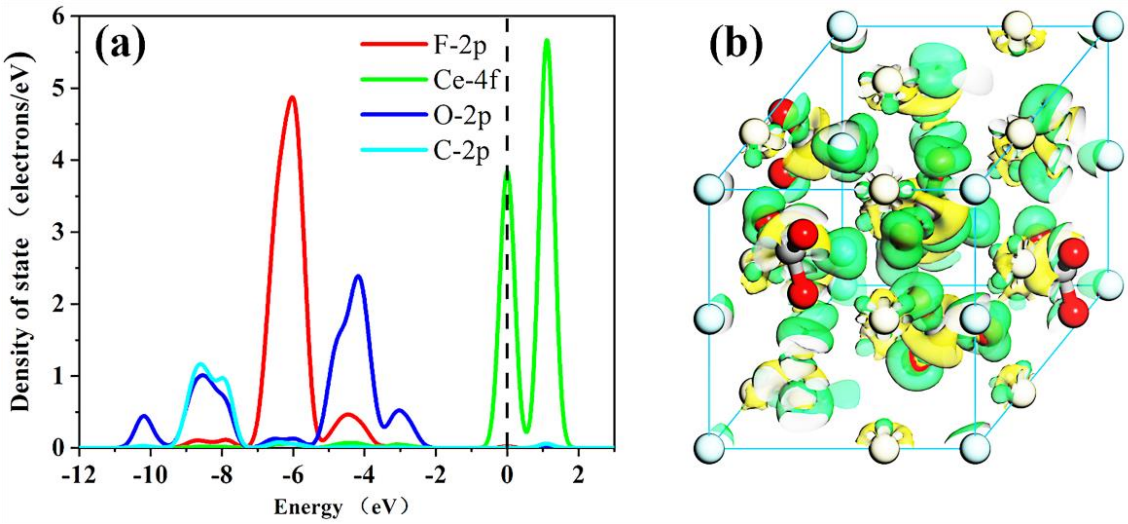

Fig. 5. (a) PDOS and (b) charge density difference of bastnaesite crystal cell (the yellow region represents charge depleption and the green region represents charge accumulation)

The forbidden band appeared below the Fermi energy level (Fig. 5(a)), indicated that bastnaesite had a semiconductor property. The electronic states near the Fermi energy level were mainly ascribed to the 4f orbital of Ce and the 2p orbital of O. In addition, the 2P orbital of C and O atoms had a more pronounced orbital hybridization peak at -8.60 eV, which further confirmed the existence of strong chemical bonds between carbon and oxygen. In addition, the same hybridization peak occurred at -4.30 eV and corresponded to the 2p orbits of F atom and C atom.

In Fig. 5(b), the yellow and green region represents the absence of charge and charge accumulation, respectively. Obviously, there was charge accumulation and charge absence between C and O atoms, indicating a strong interaction between them. Obvious charge accumulation and charge depletion respectively occurred near F and Ce atoms, indicating a strong electrostatic interaction between F and Ce atoms. Therefore, in bastnaesite crystal, C and O atoms exhibited obvious covalent bonding characteristics, whereas F and Ce atoms exhibited ionic bonding characteristics.

Mulliken charges of each atom in bastnaesite crystal were further calculated (Table 4).

Table 4. Charge transfer (Δq) of corresponding atoms in the optimized bastnaesite crystal.

Atom	Δq (e)
F	-0.53
Ce	1.70
O	-0.58
C	0.63

Obviously, F and O atoms gained electrons, whereas C and Ce atoms lost electrons (Table 4). Ce atoms lost 1.70 e of charge, indicating a significant ionic bonding feature, as shown in the above charge density difference diagram (Fig. 5(b)). The analysis results of the crystal structure and bonding characteristics of bastnaesite can be used in the selection of a suitable mineral collector.

3.2.2. Structure and adsorption properties of the (110) plane of bastnaesite crystal

When mineral crystals broke under the action of crushing and grinding force, the loss of adjacent atoms leads to an imbalance in chemical bonding force, and the chemical bonds inside the crystal were broken. The exposed atoms near the surface formed surface bond-breaking sites, resulting in the transfer of electrons near the surface and relaxation of the surface structure. During the mineral processing, freshly exposed surfaces were mainly produced in the wet grinding process.

The previous study(Chen, 2021) indicated that the (110) plane of bastnaesite crystal had a large layer spacing, the lowest bond density, and the least energy required for relaxation, so bastnaesite crystals could move most easily along the (110) plane. Therefore, the structural parameters and adsorption properties of the (110) plane of bastnaesite crystal were calculated. The structure of the (110) plane of bastnaesite crystal after geometric optimization was shown in Fig. 6. A vacuum layer larger than 20 Å was adopted in order to reduce the influences of the layer spacing on the calculation results. The bond lengths of the (110) plane of the optimized bastnaesite crystal were shown in Table 5.

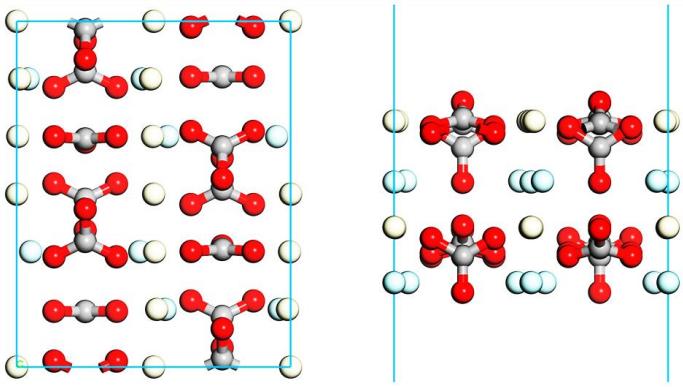

Fig. 6. Structure of the (110) plane of bastnaesite crystal after geometric optimization (Red, sky blue, grey and light yellow represent oxygen, fluorine, carbon and cerium atoms, respectively)

Table 5. Bond lengths *l* of bastnaesite crystal before and after optimization

Bastnaesite crystal	Before deconvolution (Å)	After deconvolution (Å)
$l_{F\text{-}Ce}$	2.46	2.18
$l_{O\text{-}Ce}$	2.63	2.60
$l_{F\text{-}O}$	3.20	3.78
$l_{F\text{-}C}$	3.32	3.76
$l_{C\text{-}Ce}$	3.30	3.00
$l_{O\text{-}C}$	1.30	1.30

After geometric optimization, the bond lengths of $l_{F\text{-}Ce}$, $l_{O\text{-}Ce}$ and $l_{Ce\text{-}C}$ with respect to the bulk phase decreased, but the bond lengths of $l_{F\text{-}C}$ and $l_{O\text{-}F}$ significantly increased (Table 5). This structural relaxation favored the reduction of the surface energy of solid.

The atomic structures of C_1 and C_2 were shown in Fig. 7 and the structural parameters of both collectors before adsorption are given in Table 6.

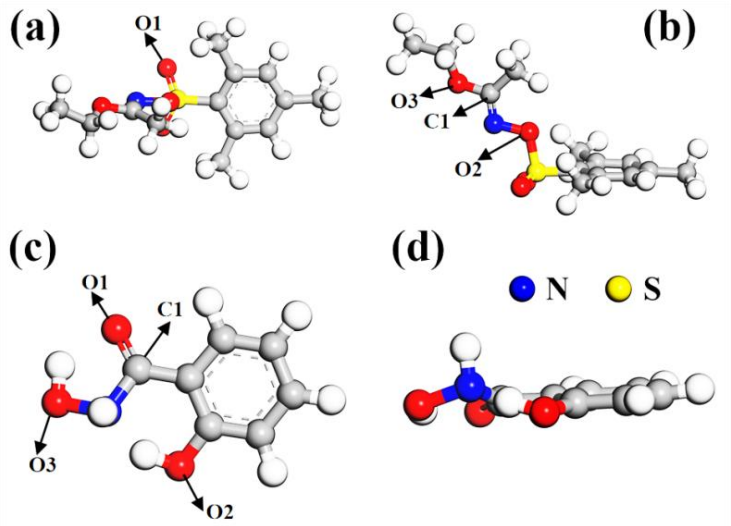

Fig. 7. Structures of optimized molecules of (a,b) C_1 and (c,d) C_2 (Red, grey, white, blue and yellow balls represent oxygen, carbon, hydrogen, nitrogen and sulfur atoms, respectively).

Table 6. Bond lengths *l* of the optimized molecules of C_1 and C_2

C_1 (Å)	Bond length	C_2 (Å)	Bond length
$l_{C\text{-}S}$	1.78	$l_{C\text{-}C_1}$	1.47
$l_{S\text{-}O_1}$	1.44	$l_{C\text{-}O_2}$	1.36
$l_{S\text{-}O_2}$	1.66	$l_{C1\text{-}O_1}$	1.24
$l_{O_2\text{-}N}$	1.45	$l_{C_1\text{-}N}$	1.41
$l_{N\text{-}C_1}$	1.30	$l_{N\text{-}O_3}$	1.41
$l_{C1\text{-}O_3}$	1.36	-	-

As shown in Fig. 7, both C_1 and C_2 molecules contain a benzene ring and three different oxygen atoms (O_1, O_2, O_3) and blue and yellow balls respectively represent N and S atoms. In order to quantitatively analyze the adsorption capacity of the two collectors on the (110) plane of bastnaesite crystal, the adsorption energy (E_b) of C_1 and C_2 molecules on the (110) plane of bastnaesite crystal is calculated as follows:

$$E_b = E_{M+CeCO_3F} - E_{CeCO_3F} - E_M \quad (1)$$

where E_{M+CeCO_3F}, E_{CeCO_3F}, and E_M denote the total energy of C_1/C_2 molecules after stable adsorption on the (110) plane of bastnaesite crystal, the total energy of the (110) plane of bastnaesite crystal and the total energy of C_1/C_2 molecules, respectively. The adsorption energy of C_1 is calculated as -1.79 eV, whereas the adsorption energy of C_2 molecule is -1.44 eV. The negative adsorption energy indicated

that the adsorption process was exothermic. The adsorption energy of C_1 was lower and the adsorption spontaneity of C_1 was stronger, indicating the stronger adsorption capacity and the better affinity of C_1 to the (110) plane of bastnaesite crystal. The result was consistent with the data obtained in the flotation test. When C_1 was used as a collector, the concentrate REO grade was 21.18% and the recovery rate was 66.78%. When C_2 was used as a collector, the concentrate REO grade was 15.36% and the recovery rate was 55.86%. Theoretical calculation results showed that the adsorption heights of C_1 and C_2 towards the (110) plane of bastnaesite crystal were respectively 1.65 Å and 2.43 Å, which were consistent with the calculation results of adsorption energy. The results proved that C_1 molecule had the better adsorption ability to the (110) plane of bastnaesite crystal.

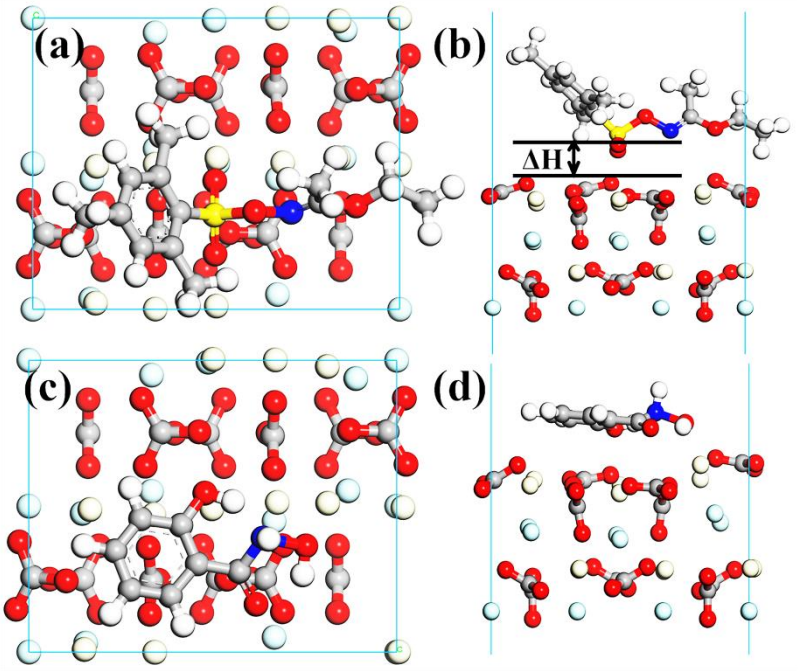

Fig. 8. Most stable structures of (a, b) C_1 and (c, d) C_2 molecules on the (110) plane of optimized bastnaesite crystal (ΔH indicates the height from the collector molecule to the (110) plane of bastnaesite crystal)(Red, grey, white, sky blue, blue and yellow balls represent oxygen, carbon, hydrogen, fluorine, nitrogen and sulfur atoms, respectively)

3.2.3. Adsorption mechanism of C_1 and C_2 molecules on the (110) plane of bastnaesite crystals

In order to investigate the effects of the molecules of two collectors on the structure of the (110) plane of bastnaesite crystal before and after the adsorption, the atomic structure diagrams of the (110) plane of bastnaesite crystal at different stages are shown in Fig. 9.

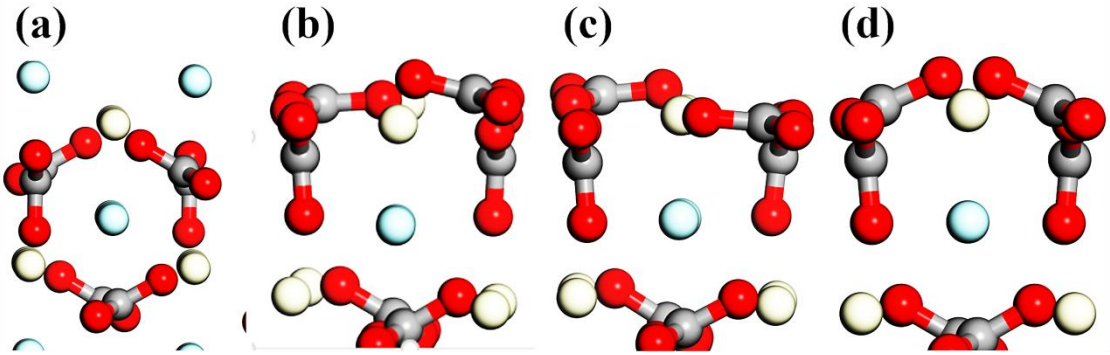

Fig. 9. Changes in the substrate in different stages: (a) pre-relaxation, (b) post-relaxation, and after adsorbing (c) C_1 molecule and (d) C_2 molecule(Red, grey, white and sky blue balls represent oxygen, carbon, hydrogen and fluorine, respectively).

A hexagon (a) formed by Ce ion surrounded by carbonate ions was gradually transformed into (c, d) irregular shapes (Fig. 9). This transformation occurred mainly on the surface layer of the (110) plane of bastnaesite crystal, indicating the strong atomic interaction between collector molecules and bastnaesite surface.

The lengths of chemical bonds between collector molecules and the (110) plane of bastnaesite crystal before and after the adsorption were provided in Tables 7 and 8.

Table 7. Bond lengths l of C_1 and C_2 molecules adsorbed on the (110) plane of bastnaesite crystal.

C_1 (Å)	Bond length	C_2 (Å)	Bond length
$l_{C\text{-}S}$	1.76	$l_{C\text{-}C1}$	1.43
$l_{S\text{-}O1}$	1.45	$l_{C\text{-}O2}$	1.38
$l_{S\text{-}O2}$	1.66	$l_{C1\text{-}O1}$	1.28
$l_{O2\text{-}N}$	1.46	$l_{C1\text{-}N}$	1.48
$l_{N\text{-}C1}$	1.30	$l_{N\text{-}O3}$	1.46
$l_{C1\text{-}O3}$	1.38	-	-

Table 8. Bond lengths l of bastnaesite crystal after adsorbing molecules.

Collector adsorption	Before adsorption (Å)	After adsorbing C_1 (Å)	After adsorbing C_2 (Å)
$l_{F\text{-}Ce}$	2.18	2.11	2.18
$l_{O\text{-}Ce}$	2.60	2.65	2.53
$l_{F\text{-}O}$	3.78	3.78	3.42
$l_{F\text{-}C}$	3.76	3.87	3.76
$l_{C\text{-}Ce}$	3.00	3.00	3.04
$l_{O\text{-}C}$	1.30	1.29	1.30

After the adsorption, the bond lengths did not change significantly, indicating that most of the collector molecules were simply adsorbed on the (110) plane of bastnaesite crystal and did not involve any chemical reaction (Tables 7 and 8). On the contrary, the structural rearrangement of the atoms on the surface of the (110) plane of bastnaesite crystal could be obviously observed. After absorbing C_2 molecule, the bond length of $l_{F\text{-}O}$ was significantly changed. In order to reveal the adsorption mechanism of C_1 and C_2 molecules on the (110) plane of bastnaesite crystal from the electronic point of view, PDOS data of both molecules and the (110) plane of bastnaesite crystal were analyzed again (Fig. 10).

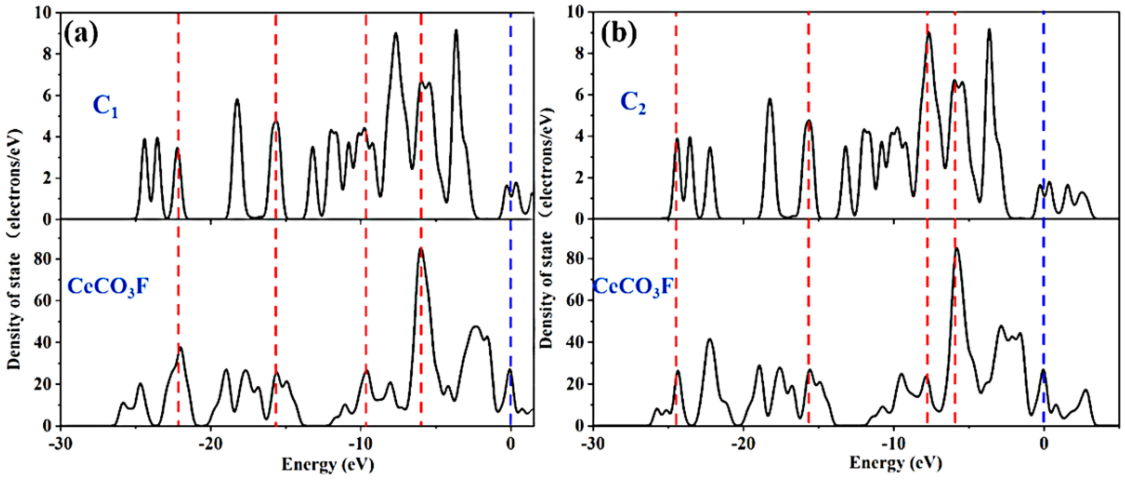

Fig. 10. PDOS analysis of C_1 and C_2 molecules adsorbed on the (110) plane of bastnaesite crystal (the Fermi energy level is set to 0 eV and the red dashed line indicates the overlapping orbital).

The C_1 molecule and the (110) plane of bastnaesite crystal underwent significant orbital hybridization at the energy density of states of -5.91 eV, -9.71 eV, -15.71 eV, and -22.18 eV (Fig. 10). As for C_2 molecule, similar hybridization peaks could be observed at -5.91 eV, -7.71 eV, -15.71 eV and -24.42

eV. The above observations indicated that the electronic interaction between collector molecules and the (110) plane of bastnaesite crystal was strong and played a crucial role in the adsorption of collector molecule.

The differential charge density maps and slices of the adsorbed molecules and the (110) plane of bastnaesite crystal are shown in Fig. 11. Yellow and blue regions represent charge reduction, and green and red regions represent charge accumulation.

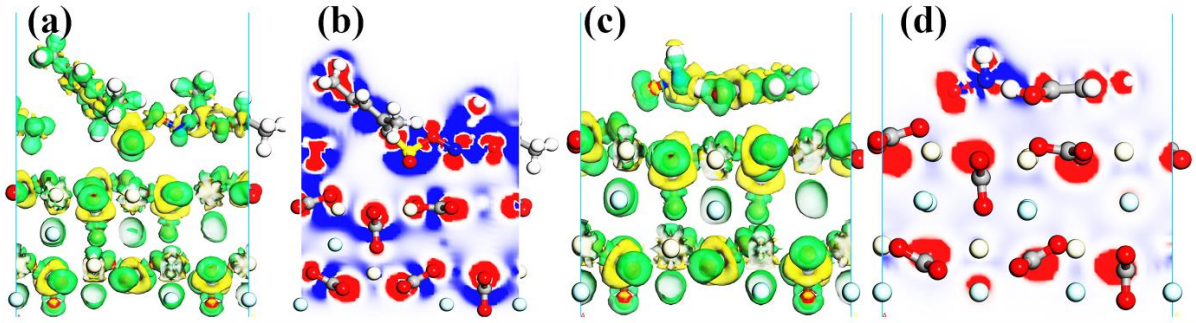

Fig. 11. Charge density difference of the most stable structures of (a, b) C_1 and (c, d) C_2 molecules on the (110) plane of optimized bastnaesite crystal as well as the structural surface analysis.

The obvious charge transfer between collector molecules (C_1 and C_2) and the substrate could be observed (Fig. 11). In addition, the Mulliken charge transfer between the molecules and the substrate was calculated (Table 9).

Table 9. Charge transfer (Δq) of corresponding atoms and molecules in bastnaesite crystals after adsorbing collector molecules.

Atom	C_1	C_2
F	-0.49	-0.52
Ce	1.69	1.86
O	-0.61	-0.62
C	0.62	0.65
Molecule	-0.46	-0.22

Note: Molecule indicates the total charge transfer of adsorbed molecules

The total charge transfer of C_1 and C_2 molecules was shown in Table 9. C_1 and C_2 molecules accepted 0.46 e^{-1} and 0.22 e^{-1} charge from the substrate, respectively. Therefore, C_1 and C_2 molecule had a stronger electrostatic interaction with the substrate, as confirmed by with the above calculated charge density results. In a word, C_1 molecule had the better selectivity and collection ability to the (110) plane of bastnaesite crystal.

4. Conclusions

In this study, with bastnaesite ore with fine mineral particles, many associated minerals, complex ore structure and difficult beneficiation as the object of research, C_1 organic molecule was firstly selected as a novel collector for bastnaesite ore from the perspective of molecular structure. Then, the comparative bastnaesite flotation test and the computation based on first principles thinking were performed between C_1 and the current industrial collector C_2. The conclusions are drawn as follows:

Firstly, the comparative flotation test showed that C_1 has better selectivity and collection ability to bastnaesite than C_2. Under the same experimental conditions, the collector C1 obtained the bastnaesite concentrate grade of 21.18% and the recovery rate of bastnaesite REO of 66.79% and the collector C_2 realized the bastnaesite concentrate grade of 15.36% and the recovery rate of 55.87%.

Secondly, the calculation results based on first principles thinking indicated that C_1 had more negative adsorption energy and lower adsorption height on the (110) plane of bastnaesite crystal than C_2. In other words, C_1 had the better affinity and stronger adsorption ability to the (110) plane of

bastnaesite crystal. PDOS calculation results showed that both collectors underwent obvious orbital hybridization on the (110) plane of bastnaesite crystal. The orbital hybridization suggested the strong electronic interaction in the adsorption process.

Thirdly, C_1 is a novel collector and has better application prospects in the industrial flotation of bastnaesite ores.

Acknowledgments

This work was supported by [Doctoral Scientific Research Foundation] grant number [YBZ202143, YBZ202221] of Xichang University and Project of Science and Technology Bureau of Liangshan Prefecture, grant number [22ZDYF0190, 21ZDYF0202] of Sichuan Province.

References

ANDERSON, C., 2021. *Beneficiation of bastnaesite ore with new flotation collector ligands*. AMMS. 7(2), 789-800.

BOLONIN, A.V., 2018. *The chemical mechanism of the formation of Fluorite-Barite-Siderite carbonatite in Karasug Fe-F-Ba-Sr-REE deposit*. Open J. Geol. 08(04), 399-403.

BOULANGER, J.-F., BAZIN, C., TURGEON, K., 2019. *Effect of depressants and temperature on bastnaesite and monazite flotation separation from a Canadian rare earth element (REE) ore*. Minerals. 9(4), 225.

CAO, S., CAO, Y., MA, Z., LIAO, Y., ZHANG, X., 2020.*Structural and electronic properties of bastnaesite and implications for surface reactions in flotation*. J. Rare Earths. 38(3), 332-338.

CHEN, J., 2021. *The interaction of flotation reagents with metal ions in mineral surfaces: A perspective from coordination chemistry*. Miner. Eng. 171, 107067.

DONNAY, G., DONNAY, J.D.H., 1953. *The crystallography of bastnaesite, parisite, roentgenite, and synchisite*. Am. Mineral.: Journal of Earth and Plane. Mater. 38(11-12), 932-963.

DUAN, H., LIU, W., WANG, X., LIU, W., ZHANG, N., ZHOU, S., 2020a. *Flotation separation of bastnaesite from calcite using novel octylmalon dihydroxamic acid as collector*. J. Mol. Liq. 312, 113484.

DUAN, H., LIU, W., WANG, X., ZHAO, L., FANG, P., GU, X., 2020b. *Preparation of a novel bis hydroxamic collector and its impact on bastnaesite flotation*. Miner. Eng. 156, 106496.

ERNZERHOF, M., PERDEW, J.P., BURKE, K., 1996. *Density functionals: Where do they come from, why do they work?* Density functional theory I: functionals and effective potentials. 1-30.

FAN, H., YANG, X., QI, J., LIU, G., QIN, J., 2021. *A comparative investigation into floatability of bastnaesite with three di/trialkyl phosphate surfactants*. J. Rare Earths. 39(11), 1442-1449.

GONG, G., LIU, J., HAN, Y., ZHU, Y., 2021. *Experimental and density functional theory studies of the effects and mechanisms of Cu2+ on flotation separation of cassiterite from fluorite*. J. Mol. Liq. 322, 114907.

GUO, C., HOU, S., WANG, W., JIN, H., 2022a. *Surface chemistry of xanthan gum interactions with bastnaesite and fluorite during flotation*. Miner. Eng. 189, 107891.

GUO, Z., KHOSO, S.A., WANG, J., ZHANG, C., GAO, Z., SUN, W., TIAN, M., LIU, Y., 2022b. *Interaction mechanism of 2-hydroxy-3-naphthyl hydroxamic acid and 1-hydroxy-2-naphthyl hydroxamic acid in the flotation separation of bastnaesite/fluorite: Experiments and first-principles calculations*. Sep. Purif. Technol. 285, 120307.

HU, W., TIAN, K., ZHANG, Z., GUO, J., LIU, X., YU, H., WANG, H., 2021. *Flotation and tailing discarding of copper cobalt sulfide ores based on the process mineralogy characteristics*. Minerals. 11(10), 1078.

JIAO, Y., QIU, K.-H., ZHANG, P.-C., LI, J.-F., ZHANG, W.-T., CHEN, X.-F., 2020. *Process mineralogy of Dalucao rare earth ore and design of beneficiation process based on AMICS*. Rare Met. 39(8), 959-966.

KANG, Y., LIU, S., 2021. *The development history and latest progress of deep-sea polymetallic nodule mining technology*. Minerals. 11(10), 1132.

LIN, Y., CHEN, C., WANG, W., JIANG, Y., CAO, X., 2020. *Beneficial effects and mechanism of lead ions for bastnaesite flotation with octyl hydroxamic acid collector*. Miner. Eng. 148, 106199.

LIU, J., PENG, B., ZHAO, L., BAI, F., LEI, Z., 2021.*Selection of an appropriate fepressant in flotation separation of molybdenum oxide from fluorapatite*. Minerals. 11(10), 1110.

LIU, P., GUO, Z., ZHANG, W., TIAN, M., SUN, W., 2024. *N-[6-(hydroxyamino)-6-oxohexyl]octanamide: A collector derived from the structure of octyl hydroxamic acid and its application in bastnaesite flotation*. Sep. Purif. Technol. 331, 125562.

LIU, T., CHEN, J., 2021. *Extraction and separation of heavy rare earth elements: A review*. Sep. Purif. Technol. 276, 119263.

LIU, W., MCDONALD, L.W., WANG, X., MILLER, J.D., 2018. *Bastnaesite flotation chemistry issues associated with alkyl*

phosphate collectors. Miner. Eng. 127, 286-295.

LIU, W., WANG, X., MILLER, J.D., 2019. *Collector chemistry for bastnaesite flotation – recent developments*. Miner. Process. Extr. Metall. Rev. 40(6), 370-379.

LIU, W., WANG, X., WANG, Z., MILLER, J.D., 2016. *Flotation chemistry features in bastnaesite flotation with potassium lauryl phosphate*. Miner. Eng. 85, 17-22.

NI, Y., HUGHES, J.M., MARIANO, A.N., 1993.*The atomic arrangement of bastnäesite-(Ce), Ce (CO3) F, and structural elements of synchysite-(Ce), röntgenite-(Ce), and parisite-(Ce)*. Am. Mineral. 78(3-4), 415-418.

NIE, Q., WANG, M., QIU, T., QIU, X., 2020.*Density functional theory and XPS studies of the adsorption of cyanide on chalcopyrite surfaces*. ACS omega. 5(36), 22778-22785.

PARK, I., KANAZAWA, Y., SATO, N., GALTCHANDMANI, P., JHA, M.K., TABELIN, C.B., JEON, S., ITO, M., HIROYOSHI, N., 2021.*Beneficiation of low-grade rare earth ore from khalzan buregtei deposit (Mongolia) by magnetic separation*. Minerals. 11(12), 1432.

QUEZADA, G.R., TOLEDO, P.G., 2019.*Structure of the interface between lithium-rich spodumene and saltwater by density functional theory calculations and molecular dynamics Simulations*. J. Phys. Chem. C. 124(2), 1446-1457.

REPUB, S.A.O.T.P.S., REGULATION, S.A.F.M., 2020. *Rare earth metals and their compounds-Determination of total rare earth contents*, In *National Standards of the People's Republic of China*, ed. REPUB, S.A.O.T.P.S. Standards Press of China, China, pp. 1-11.

SAHRAEI, A.A., LARACHI, F., 2020. *How do surface defects change local wettability of the hydrophilic ZnS surface? Insights into sphalerite flotation from density functional theory calculations*. J. Phys. Chem. C. 125(1), 998-1009.

SEGALL, M.D., LINDAN, P.J.D., PROBERT, M.J., PICKARD, C.J., HASNIP, P.J., CLARK, S.J., PAYNE, M.C., 2002. *First-principles simulation: ideas, illustrations and the CASTEP code[J]., 2002, 14(11): 2717.* J. Phys.: Condens.Matter. 14(11), 2717.

SUN, X., WU, B., HU, M., QIU, H., DENG, J., CAI, J., JIN, X., 2021. *Flotation depression of arsenopyrite using sodium nitrobenzoate under alkaline conditions*. Minerals. 11(11), 1216.

WANG, C., SHI, H., QIU, X., HU, Z., 2020a. *Difference in flotation behavior between fine-grained bastnaesite and barite*. J. Chin. Soc. Rare Earths. 38(6), 816-822.

WANG, D., LIU, D., MAO, Y., SUN, R., LIU, R., WEN, S., 2021. *Effect of fluoride ion on the separation of fluorite from calcite using flotation with acidified water glass*. Minerals. 11(11), 1203.

WANG, J., ZU, P., YI, S., CAO, Z., 2020b. *Preconcentration of iron, rare earth, and fluorite from bayan obo ore using superconducting magnetic separation*. Mining. Metall. Explor. 38(2), 701-712.

WANG, W., LI, E., PENG, Z., GUO, C., HOU, S., LI, Q., 2023. *Flotation separation of bastnaesite from monazite using depressant dextrin hydrate and its depression mechanism*. Miner. Eng. 200, 108151.

WANG, Z., WU, H., XU, Y., SHU, K., FANG, S., XU, L., 2020c. *The effect of dissolved calcite species on the flotation of bastnaesite using sodium oleate*. Miner. Eng. 145, 106095.

WANG, Z., WU, H., XU, Y., SHU, K., YANG, J., LUO, L., XU, L., 2020d. *Effect of dissolved fluorite and barite species on the flotation and adsorption behavior of bastnaesite*. Sep. Purif. Technol. 237, 116387.

WANG, Z., WU, H., YANG, J., TANG, Z., LUO, L., SHU, K., XU, Y., XU, L., 2020e. *Selective flotation separation of bastnaesite from calcite using xanthan gum as a depressant*. Appl. Surf. Sci. 512, 145714.

XIONG, W., DENG, J., CHEN, B., DENG, S., WEI, D., 2018. *Flotation-magnetic separation for the beneficiation of rare earth ores*. Miner. Eng. 119, 49-56.

XU, L., WANG, Z., SHU, K., WU, H., HU, Y., 2022. *Surface chemistry considerations of gangue dissolved species in the bastnaesite flotation system*. Fundam. Res. 2(5), 748-756.

XU, Y., XU, L., WU, H., TIAN, J., WANG, Z., GU, X., 2020a. *The effect of citric acid in the flotation separation of bastnaesite from fluorite and calcite using mixed collectors*. Appl. Surf. Sci. 529, 147166.

XU, Y., XU, L., WU, H., WANG, Z., SHU, K., FANG, S., ZHANG, Z., 2020b. *Flotation and co–adsorption of mixed collectors octanohydroxamic acid/sodium oleate on bastnaesite*. J. Alloys Compd. 819, 152948.

Y., Z., W., Y., 1998.*Comment on "Generalized gradient approximation made simple"*. Phys. Rev. Lett. 80(4), 890.

YAO, J., SUN, H., BAN, X., YIN, W., 2021. *Analysis of selective modification of sodium dihydrogen phosphate on surfaces of magnesite and dolomite: Reverse flotation separation, adsorption mechanism, and density functional theory calculations*. Colloids Surf., A. 618, 126448.

YU, Q., TIAN, F., CAO, Y., FAN, G., HAO, H., PENG, W., ZHOU, G., LI, P., 2021. *Application of Waste Engine Oil for Improving Ilmenite Flotation Combined with Sodium Oleate Collector*. Minerals. 11(11), 1242.

ZHANG, C., ZHU, X., PENG, C., GUO, C., 2022. *Adsorption of rare earth La^{3+} by a- zirconium phosphate: An experimental*

and density functional theory study. Journal of Molecular Liquids. 368, 120668.

ZHANG, Q., NIU, C., BU, X., BILAL, M., NI, C., PENG, Y., 2021. *Enhancement of Flotation Performance of Oxidized Coal by the Mixture of Laurylamine Dipropylene Diamine and Kerosene*. Minerals. 11(11), 1271.

ZHOU, H., LIU, S., YI, H., SONG, S., JIA, F., 2023. *Flotation of bastnaesite by mixed collectors and adsorption mechanism*. Chem. Phys. Lett. 830, 140793.

ZHU, X., LIN, Y., HUANG, Y., ZHU, Y., SHI, C., WANG, W., 2020. *Adsorption of ferric ions on the surface of bastnaesite and its significance in flotation*. Miner. Eng. 158, 106588.